Electronic Supplementary Information

Atmosphere-Directed Reconstruction of Cu-based Metal-Organic Frameworks toward Efficient CO_2 Electroreduction

Jiye Feng,[‡a] Danni Shi,[‡a] Fei Wang,[a] Yiming Zou,[a] Weicheng Li,[a] Wenbiao Zhang,[a] Huaijun Lin,[a] Yuying Meng,[a] and Qingsheng Gao[*a]

[a] College of Chemistry and Materials Science, Guangdong Provincial Key Laboratory of Functional Supramolecular Coordination Materials and Applications, Jinan University, Guangzhou 510632, P. R. China. E-mail: tqsgao@jnu.edu.cn

[‡] These authors contributed equally to this work.

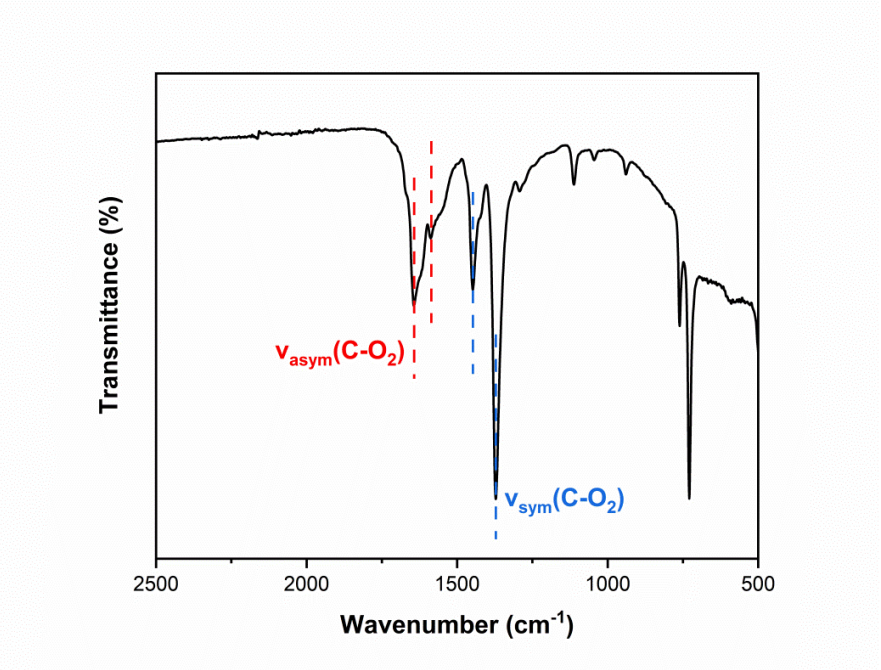

Fig. S1. FT-IR spectra of HKUST-1.

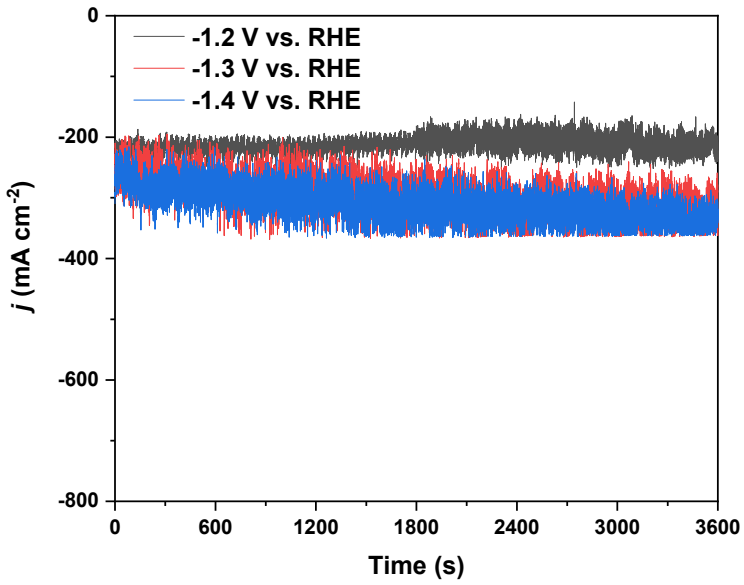

Fig. S2. Chronoamperometry curve of HKUST-1 during the *in situ* electrochemical reconstruction at various potentials.

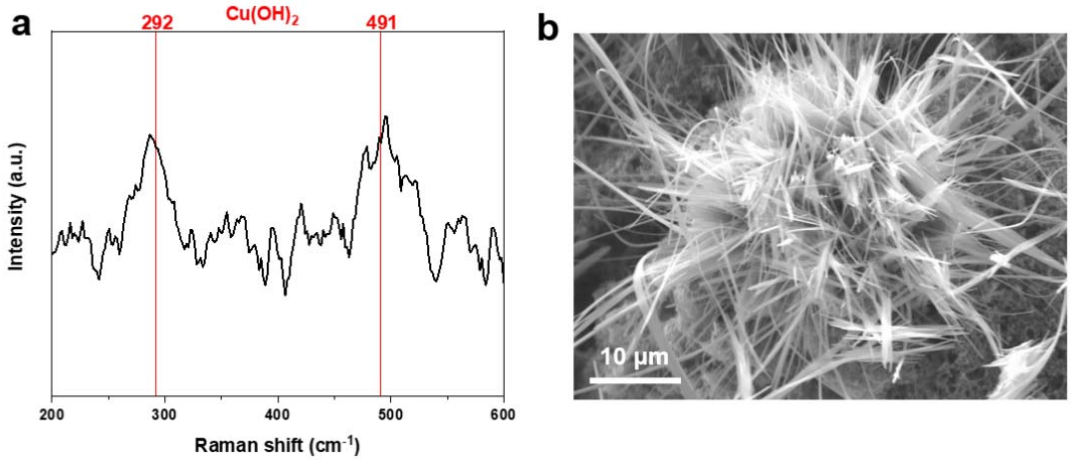

Fig. S3. (a) Raman spectra and (b) SEM image of HKUST-1 after soaking with 1.0 M KOH for 1 h under Ar atmosphere without applied potentials.

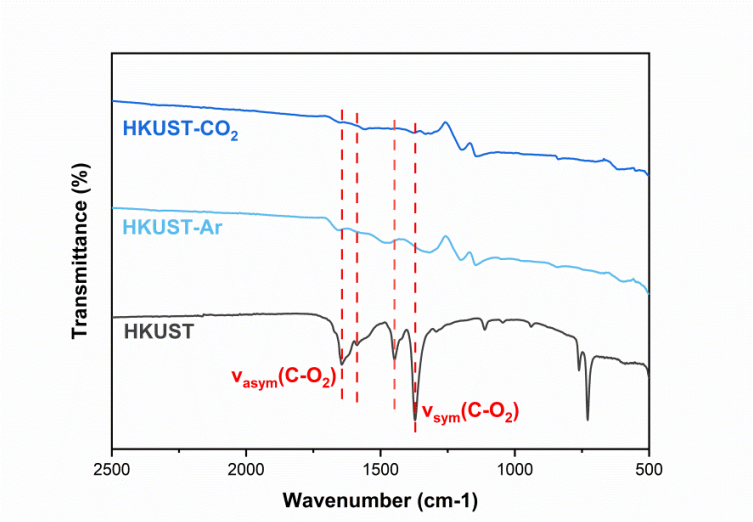

Fig. S4. FTIR spectra of the restructured HKUST-CO_2 and HKUST-Ar.

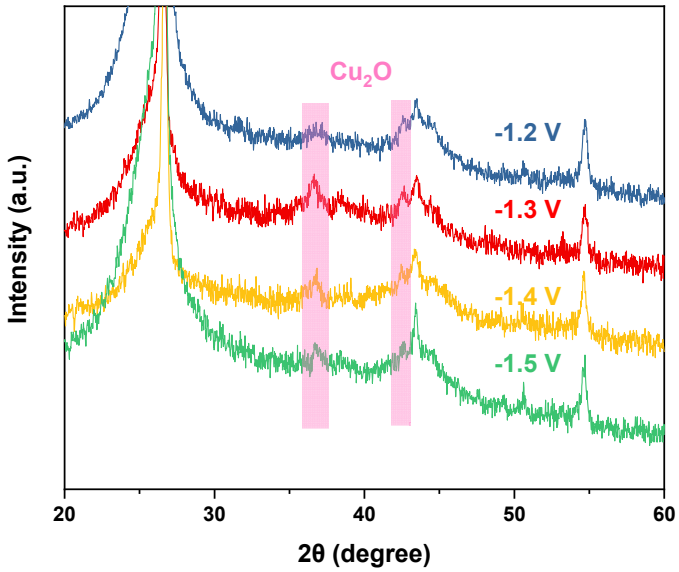

Fig. S5. *Ex situ* XRD patterns of HKUST-Ar collected at different potentials.

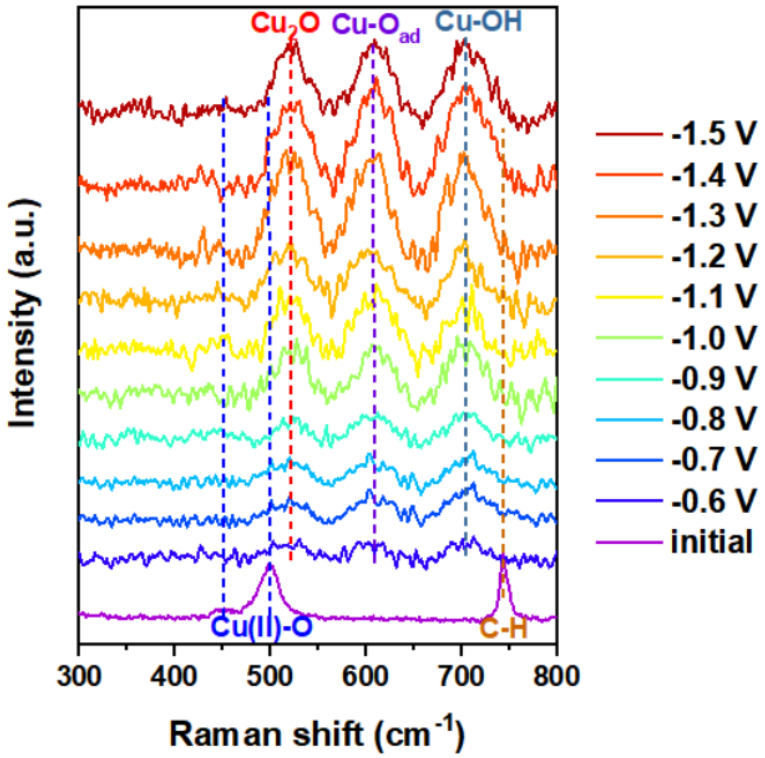

Fig. S6. *In situ* Raman spectra of HKUST-Ar collected at different potentials.

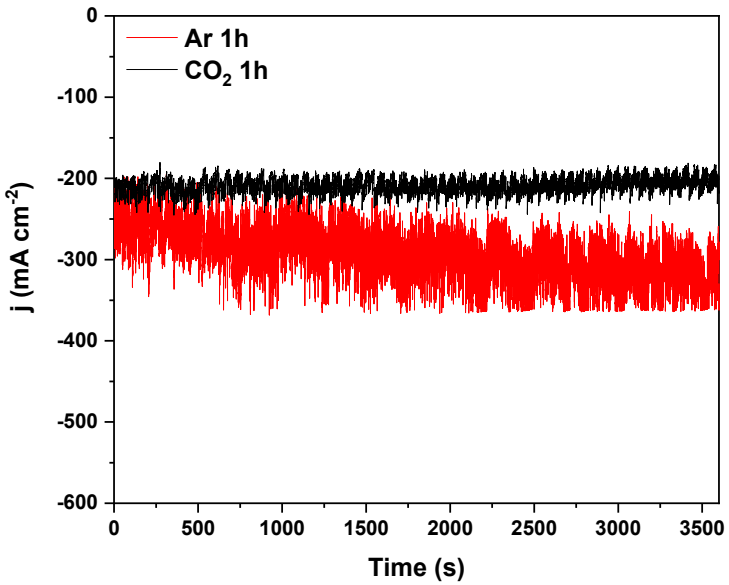

Fig. S7. Chronoamperometry curves of HKUST-1 reconstructed in Ar and CO_2 atmospheres at -1.3 V (vs. RHE).

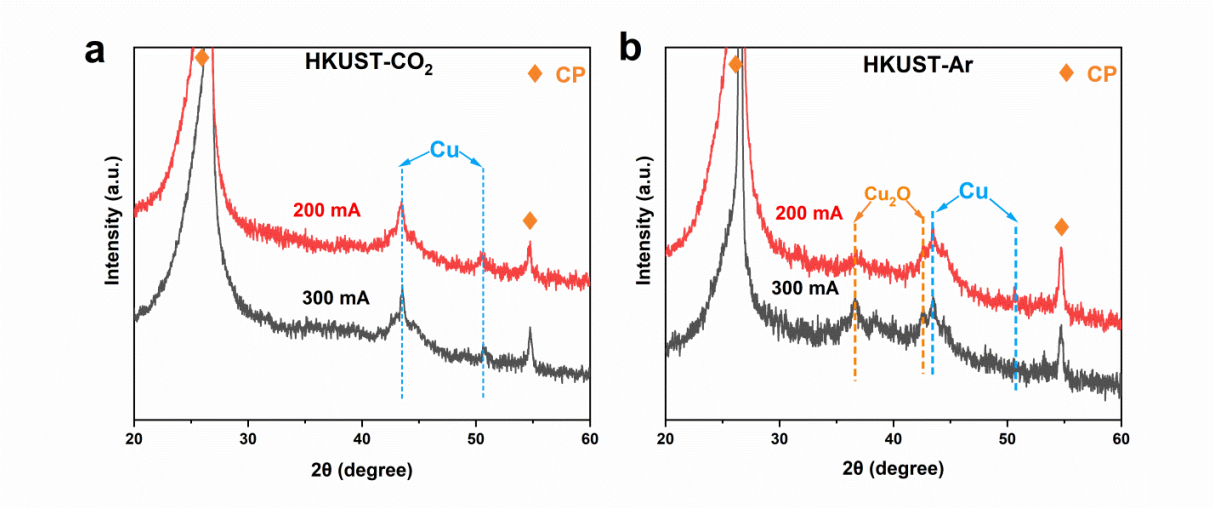

Fig. S8. XRD patterns of HKUST-1 reconstructed in (a) CO_2 and (b) Ar at j = -200 and -300 mA cm^{-2}.

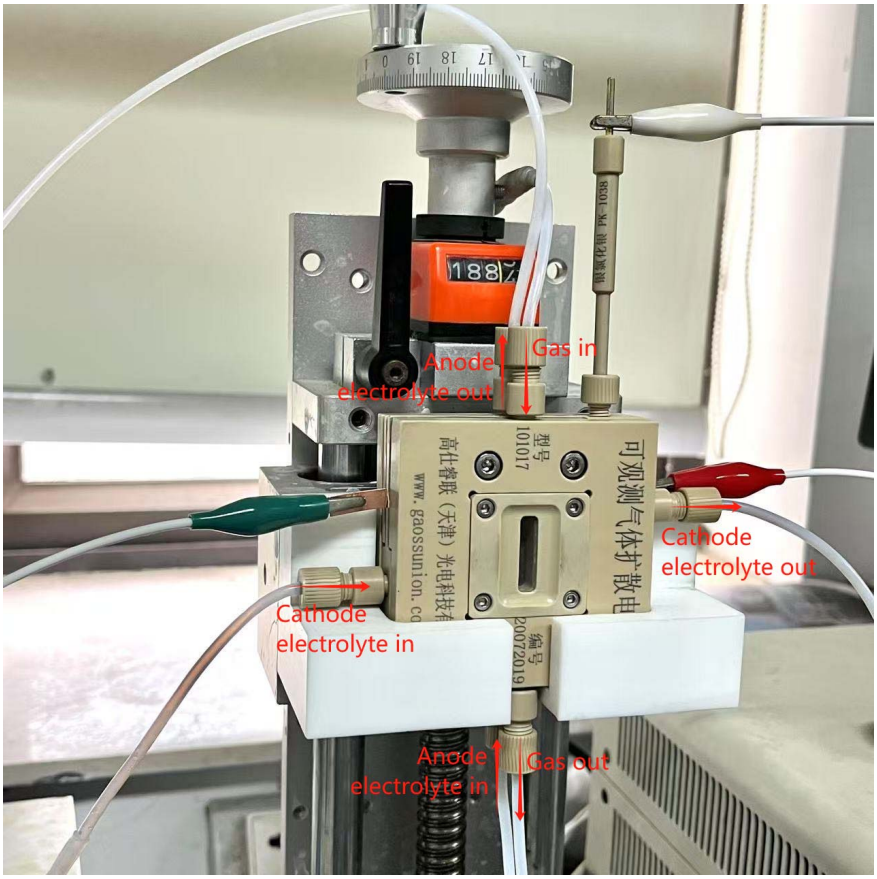

Fig. S9. The photograph of the flow cell used for CO_2RR.

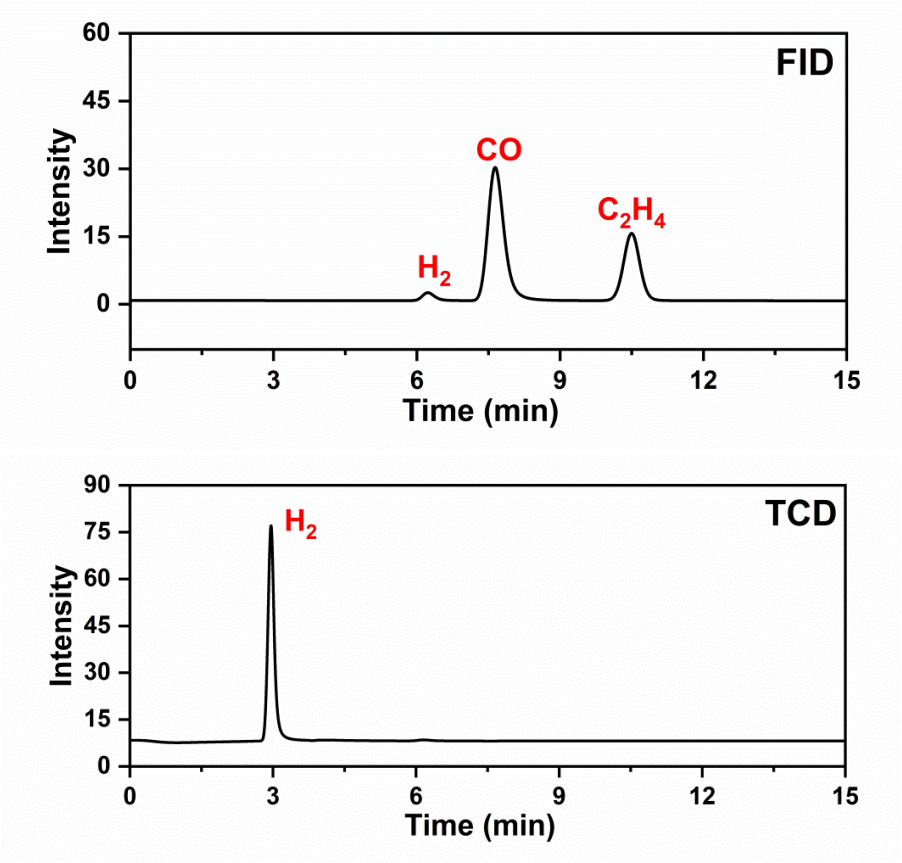

Fig. S10. Representative gas chromatography (GC) spectra of the gas products.

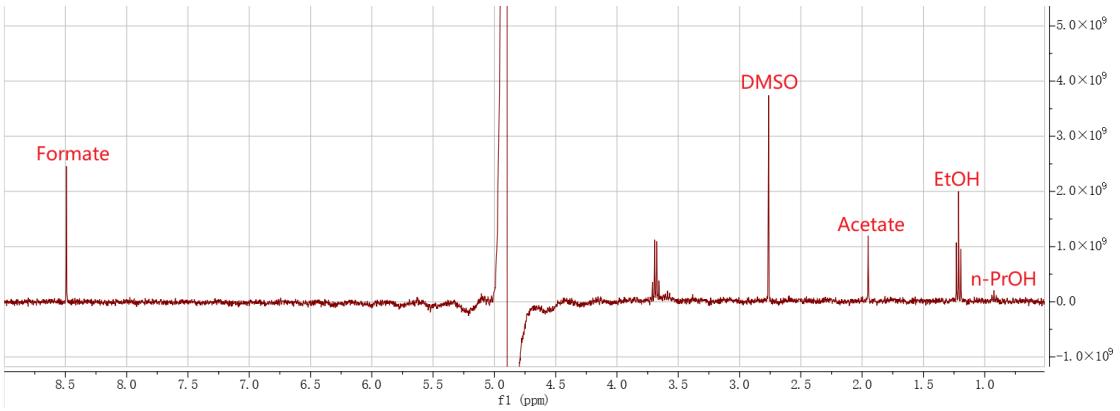

Fig. S11. Representative nuclear magnetic resonance (NMR) spectra of the liquid products.

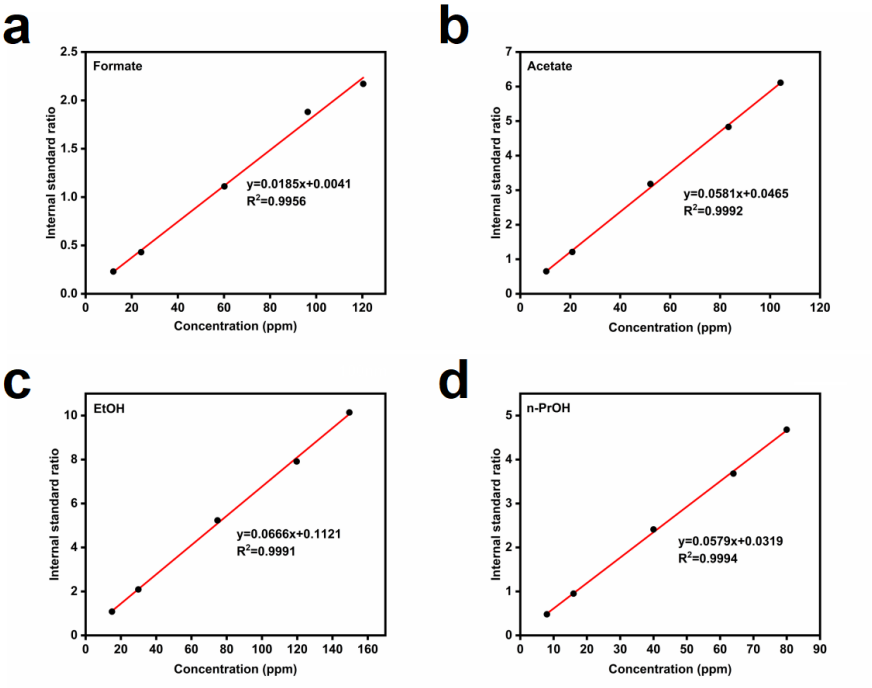

Fig. S12. Standard curves for analyzing liquid products on ^{1}H NMR.

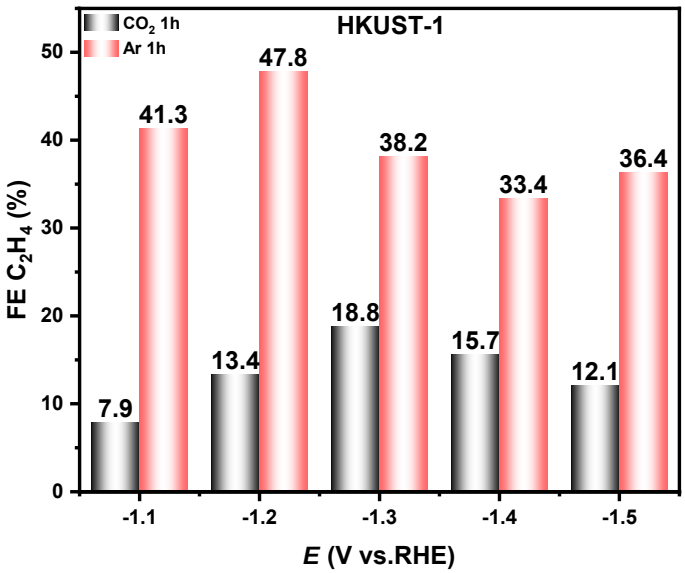

Fig. S13. FE of C_2H_4 on HKUST-CO_2 and HKUST-Ar for the CO_2RR at different applied potentials.

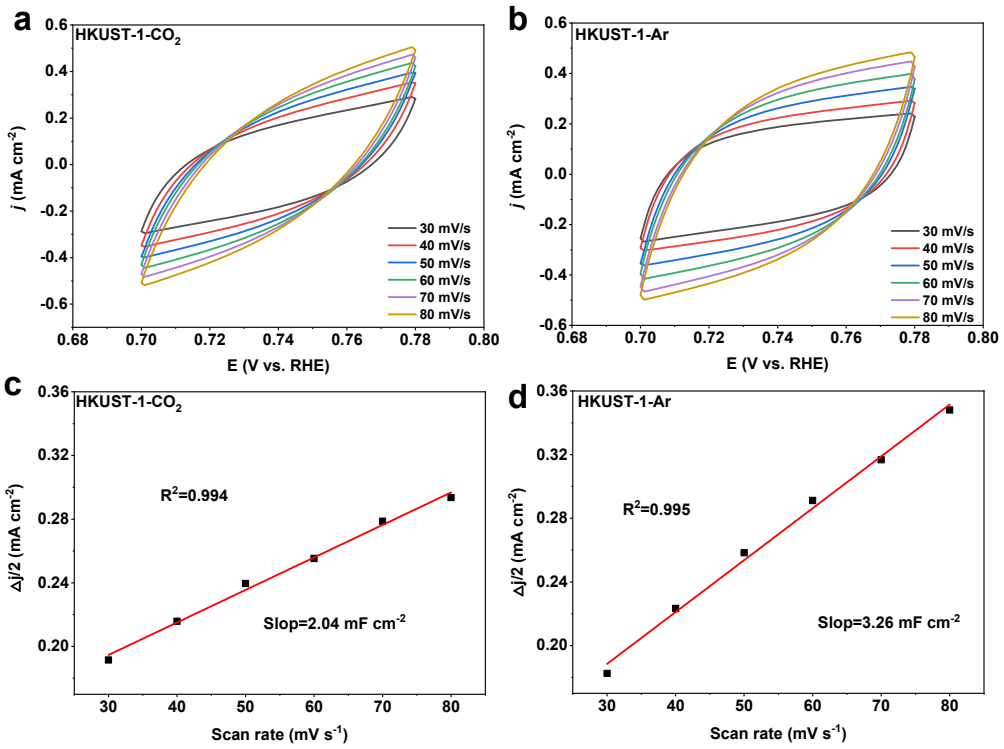

Fig. S14. (a-b) CVs with various scan rates of HKUST-CO_2 and HKUST-Ar. (c-d) Current due to double-layer charging plotted against scan rates of HKUST-CO_2 and HKUST-Ar.

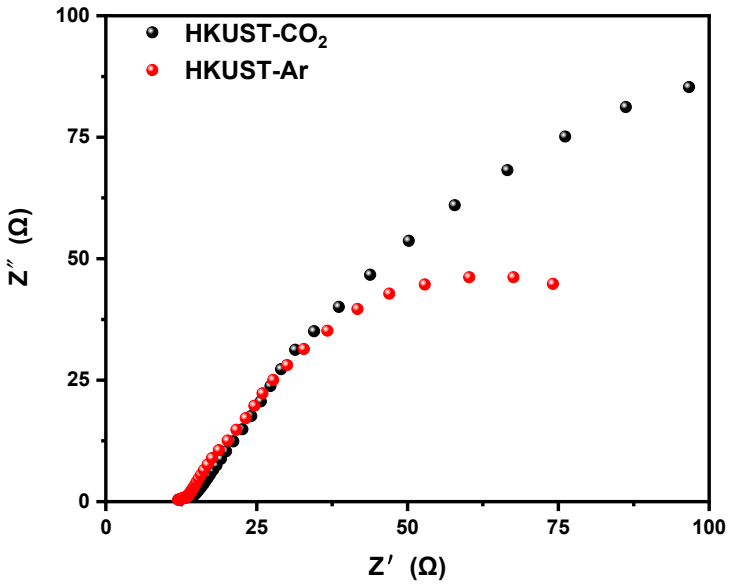

Fig. S15. EIS spectra of HKUST-CO_2 and HKUST-Ar in 1.0 M KOH at -1.0 V vs. RHE, measured over the frequency range of 0.1 Hz to 100 kHz.

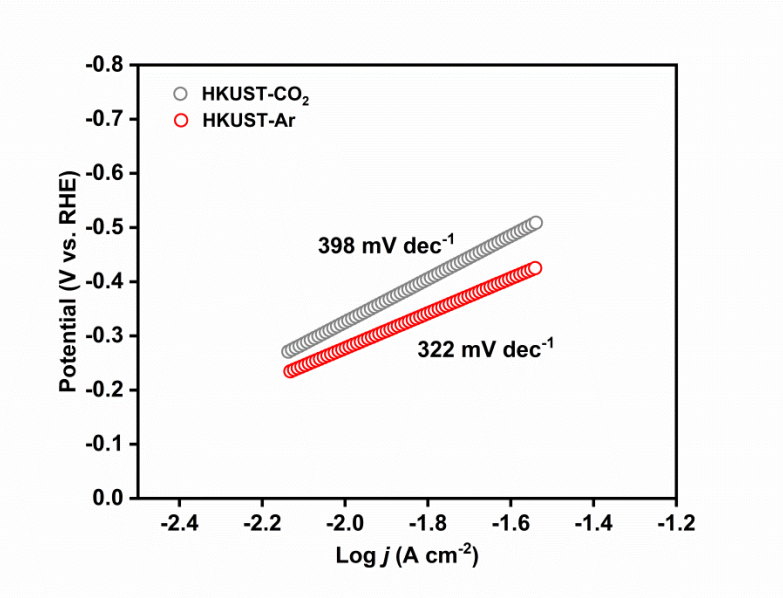

Fig. S16. Tafel slopes of HKUST-CO_2 and HKUST-Ar in flow cell.

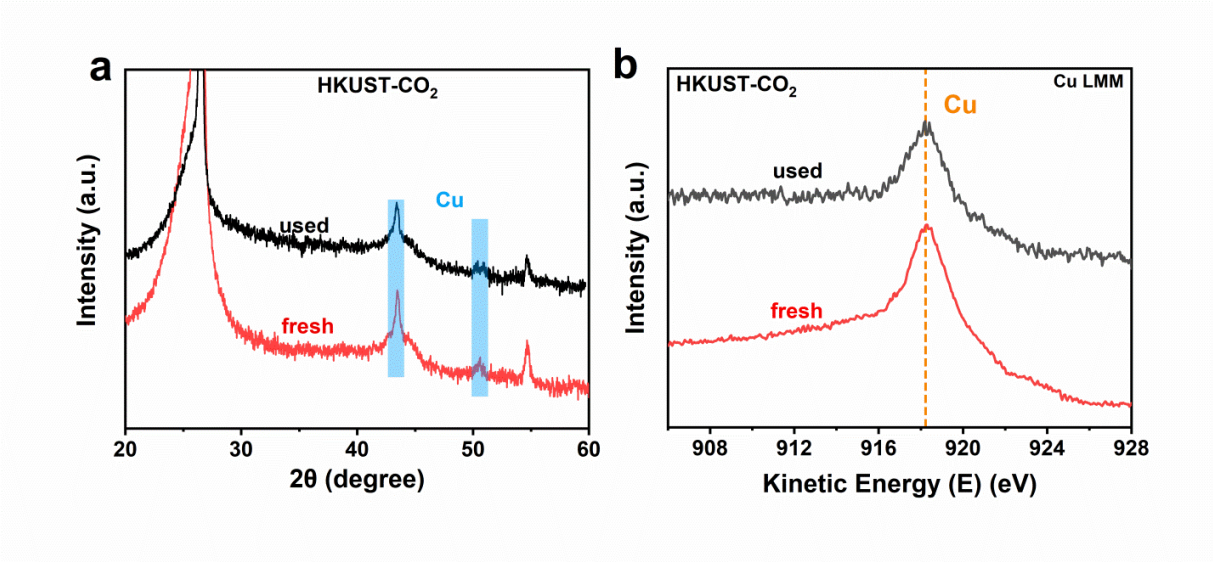

Fig. S17. (a) XRD patterns and (b) Cu LMM AES of HKUST-CO_2 before and after CO_2RR.

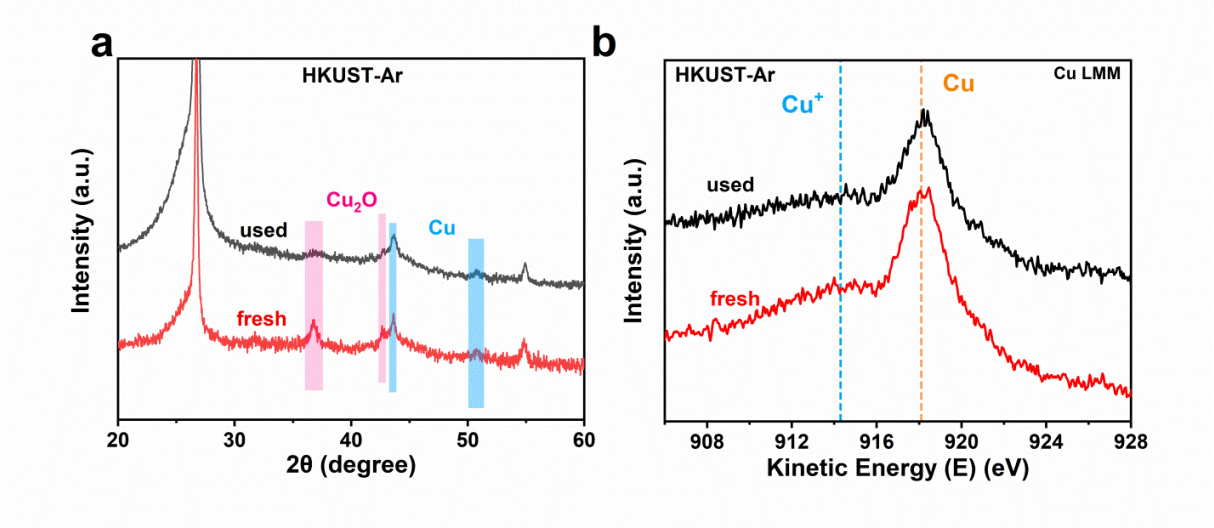

Fig. S18. (a) XRD patterns and (b) Cu LMM AES of HKUST-Ar before and after CO_2RR.

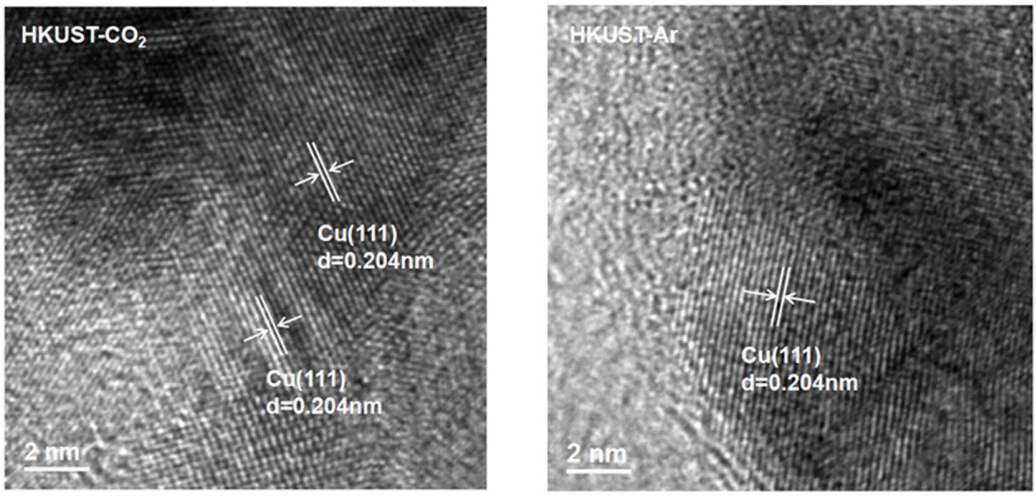

Fig. S19. HR-TEM images of HKUST-CO_2 and HKUST-Ar after CO_2RR test.

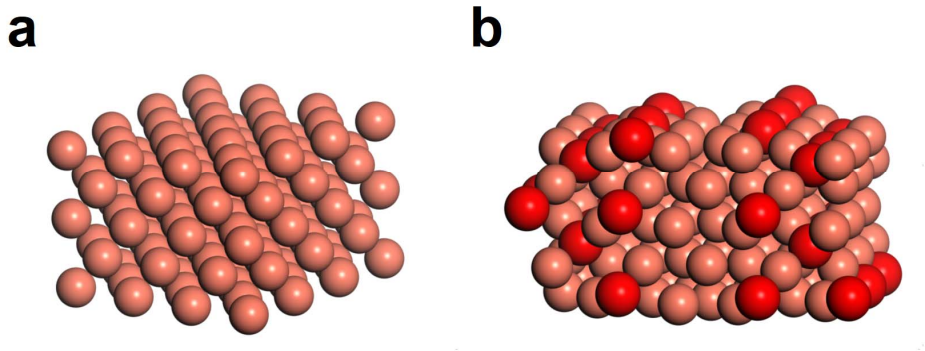

Fig. S20. The structural models of (a) Cu and (b) Cu/Cu_2O. Color code: Cu, orange; O, red.

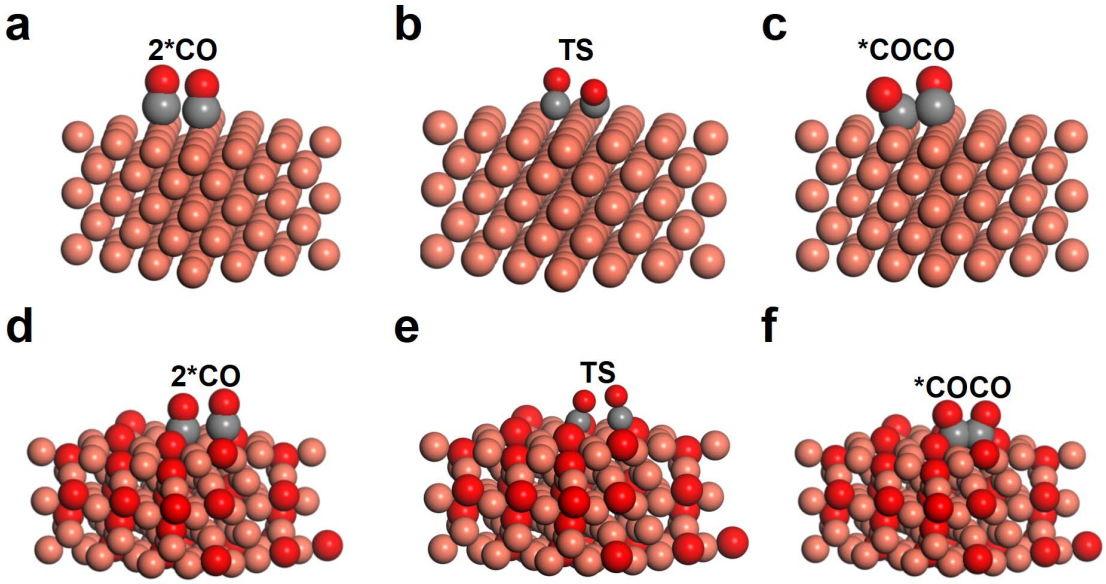

Fig. S21. The initial states, transition states and final states of *CO-*CO coupling on (a-c) Cu and (d-f) Cu/Cu_2O models. Color code: Cu, orange; C, gray; O, red.

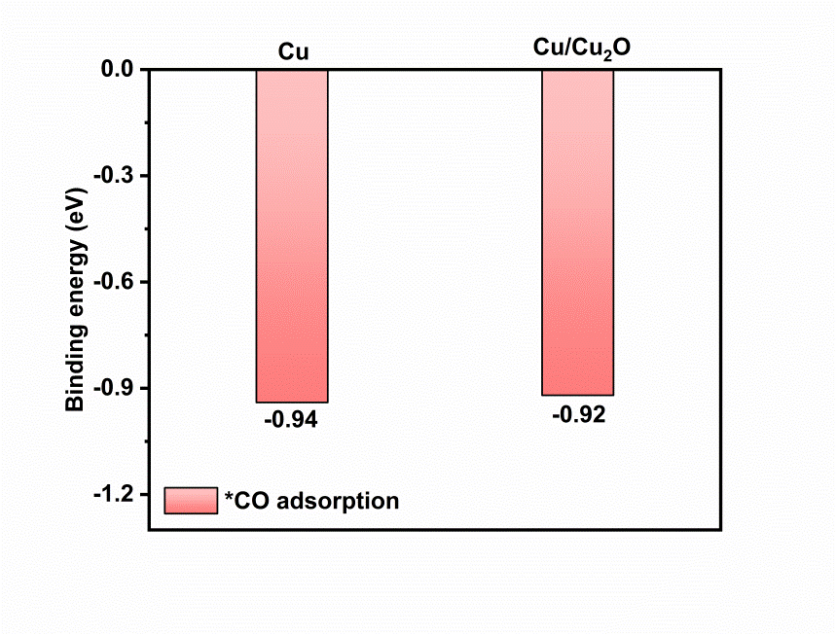

Fig. S22. Energy profiles of *CO adsorption on Cu and Cu/Cu_2O.

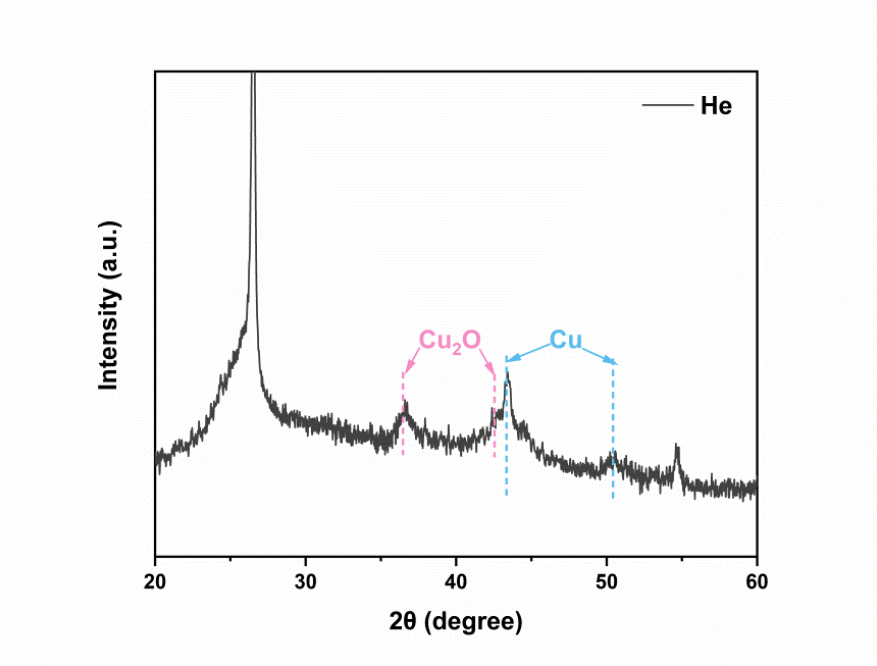

Fig. S23. XRD pattern of HKUST-He.

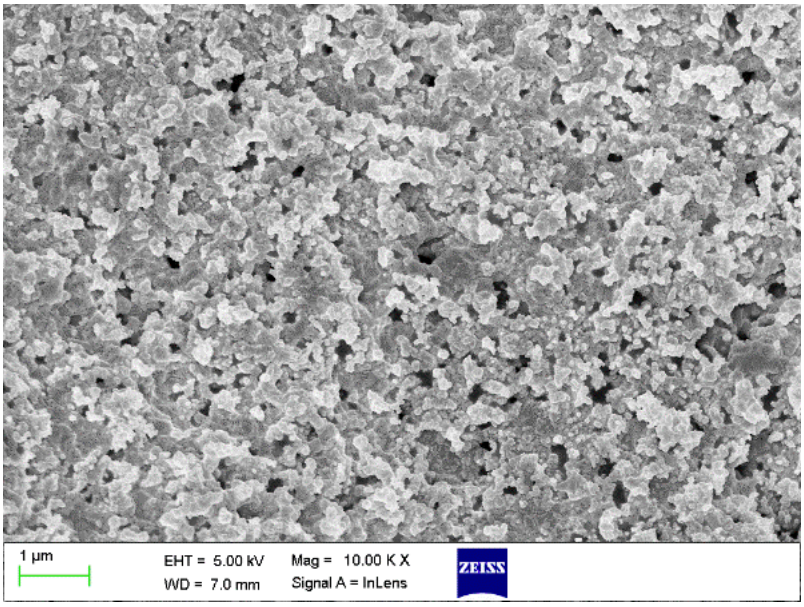

Fig. S24. SEM image of HKUST-He.

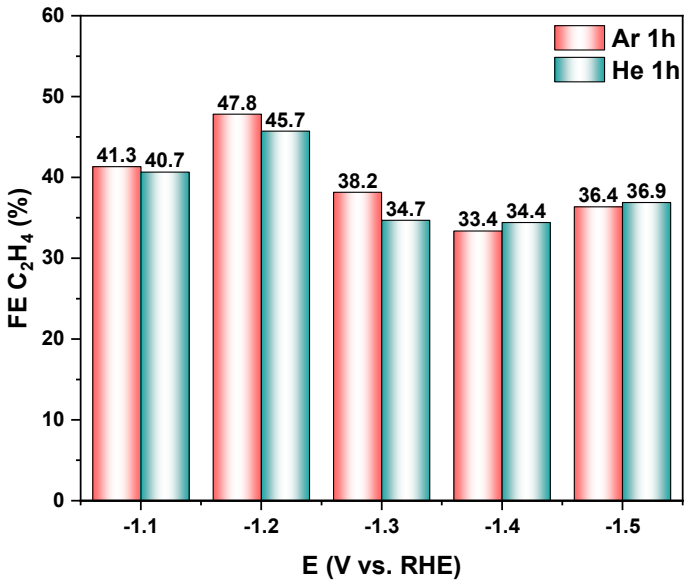

Fig. S25. FE of C_2H_4 at different applied potentials of HKUST-He and HKUST-Ar.

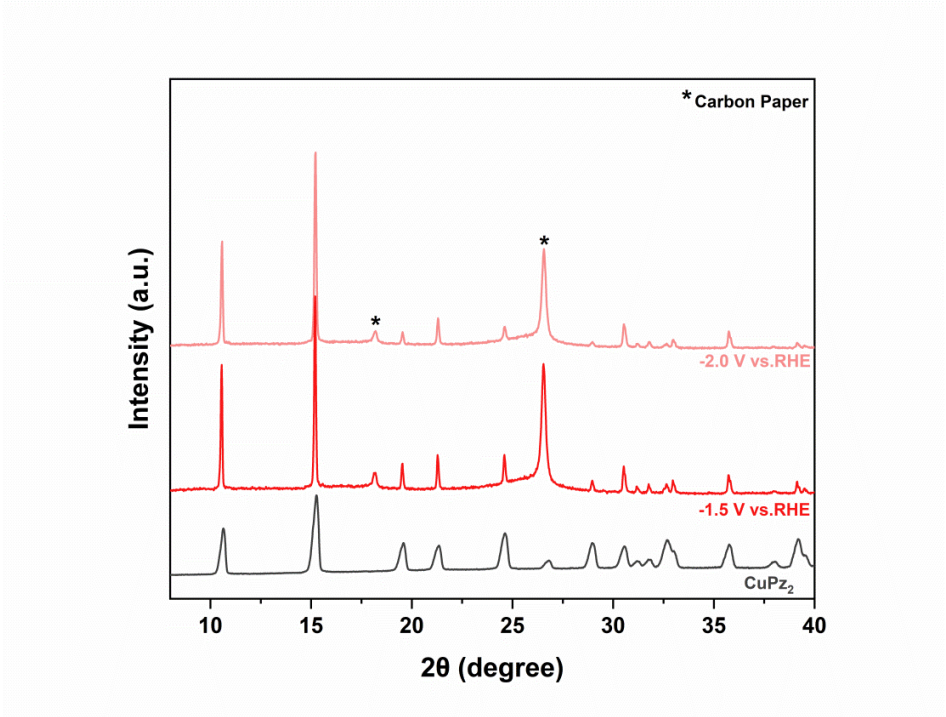

Fig. S26. XRD patterns of $CuPz_2$ under Ar atmosphere at different potentials.

Table S1. FEs of different liquid products on HKUST-Ar.

Products	internal standard ratio	Concentration (ppm)	FE (%)
Formate	0.53	28.43	1.65
Acetate	0.36	5.40	0.96
EtOH	1.13	15.28	5.32
n-PrOH	0.18	2.56	1.03

Table S2. Calculated energy, entropy, zero-point energy correction and Gibbs free energy for C-C coupling on Cu and Cu/Cu_2O.

	ΔE (eV)	T***Δ**S (eV)	**Δ**ZPE (eV)	**Δ**G (eV)
Cu	-1.84	-0.7	1.3	0.16
Cu/Cu_2O	-1.88	-0.84	0.9	-0.14